Supporting Information for:

Synthesis of doubly thermo-responsive schizophrenic diblock copolymer based on poly[*N*-(4-vinylbenzyl)-*N*,*N*-diethylamine] and its temperature-sensitive flip-flop micellization

Shentong Li, Fei Huo, Quanlong Li, Chengqiang Gao, Yang Su and Wangqing Zhang*

Key Laboratory of Functional Polymer Materials of the Ministry of Education, Collaborative Innovation Center of Chemical Science and Engineering (Tianjin), Institute of Polymer Chemistry, Nankai University, Tianjin 300071, China.

* To whom correspondence should be addressed. E-mail: wqzhang@nankai.edu.cn, Tel: 86-22-23509794, Fax: 86-22-23503510.

1. The chemical structure of VEA and CDTPA.

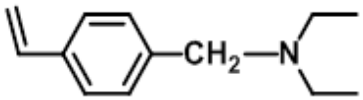

Scheme S1. The chemical structure of VEA.

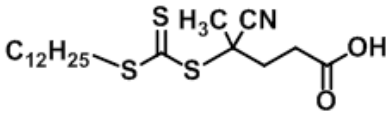

Scheme S2. The chemical structure of CDTPA.

2. The ^{1}H NMR spectrum of VEA

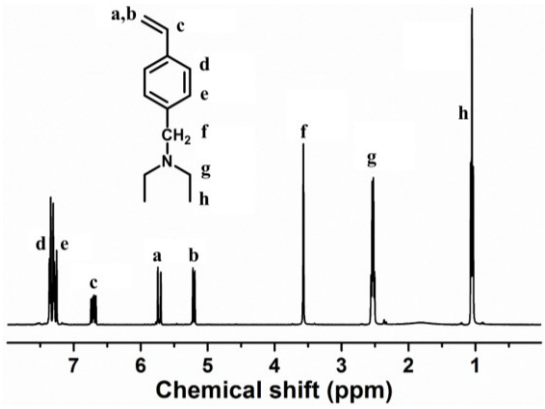

Fig. S1. The ^{1}H NMR spectrum of VEA.

3. Synthesis and characterization of PVEA$_{133}$ by RAFT polymerization

Into a Schlenk flask, VEA (1.419 g, 7.5 mmol), CDTPA (12.1 mg, 0.030 mmol), AIBN (1.64 mg, 0.010 mmol) dissolved in 1,4-dioxane (0.50 g) and the internal standard of 1,3,5-trioxane (67.6 mg, 0.75 mmol) were added. The solution was initially degassed with nitrogen at 0 ^{o}C for 30 min, and then the flask content was immersed into a preheated oil bath at 70 ^{o}C. After 16 h, the reaction was quenched by cooling to 0 ^{o}C, and an aliquot was withdrawn to determine the monomer conversion by ^{1}H NMR analysis. The VEA monomer conversion was calculated according to eq 2. The synthesized polymer was precipitated in the ethanol/water mixture (6/5 by weight) and dried at room temperature under vacuum.

4. The ^{1}H NMR spectra of PVEA$_{133}$

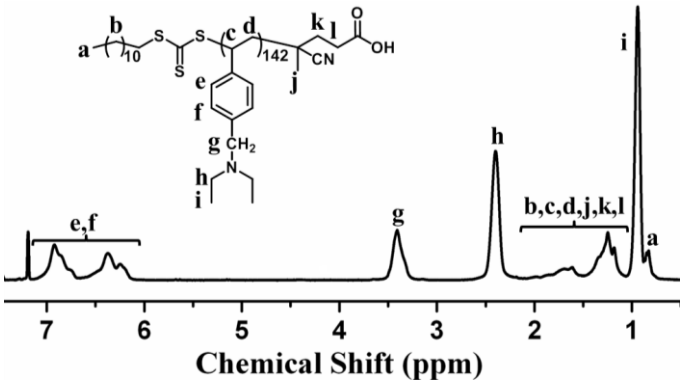

Fig. S2. The ^{1}H NMR spectra of PVEA$_{133}$.

5. The GPC traces of PVEA$_{133}$, P*t*BMA$_{136}$, P*t*BMA$_{217}$, and P*t*BMA$_{329}$

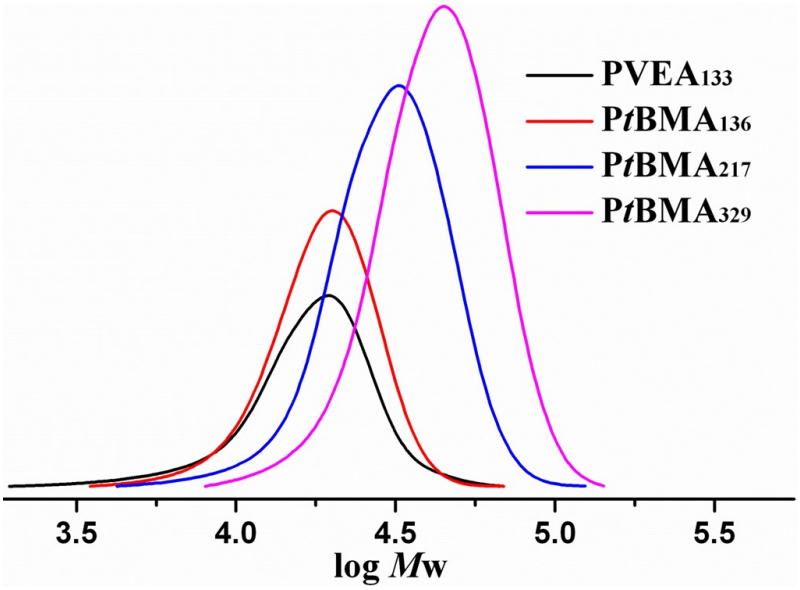

Figure S3. The GPC traces of PVEA$_{133}$, P*t*BMA$_{136}$, P*t*BMA$_{217}$, and P*t*BMA$_{329}$.

6. The transmittance versus temperature plots for PVEA$_{133}$, P*t*BMA$_{136}$, P*t*BMA$_{217}$, and P*t*BMA$_{329}$

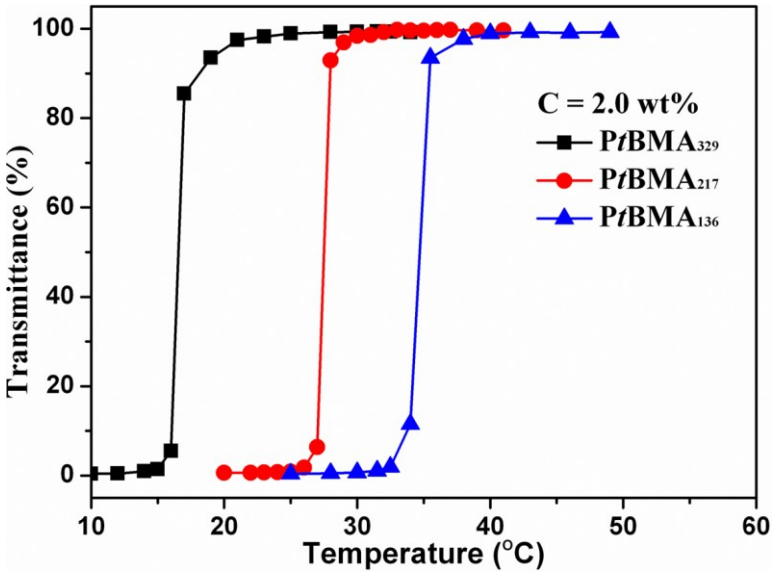

Fig. S4. The transmittance versus temperature plots for PVEA$_{133}$, P*t*BMA$_{136}$, P*t*BMA$_{217}$, and P*t*BMA$_{329}$.

7. High-resolution digital photographs of P*t*BMA$_{329}$-*b*-P*t*BMA$_{142}$ in methanol

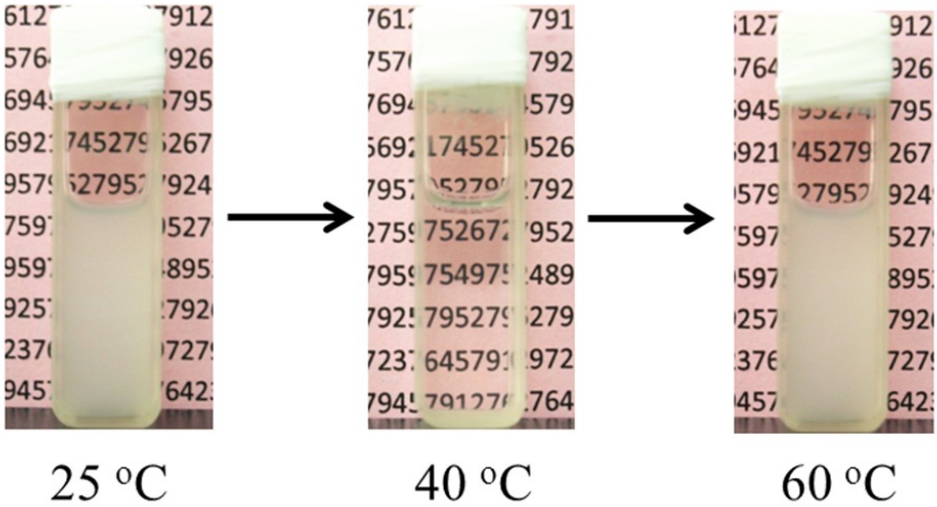

Fig. S5. The high-resolution digital photographs of P*t*BMA$_{329}$-*b*-P*t*BMA$_{142}$ in methanol at different temperature, in which the polymer concentration is 2.0 wt%.

8. Polymer concentration affecting LCST/UCST of P*t*BMA$_{329}$-*b*-P*t*BMA$_{142}$ in methanol

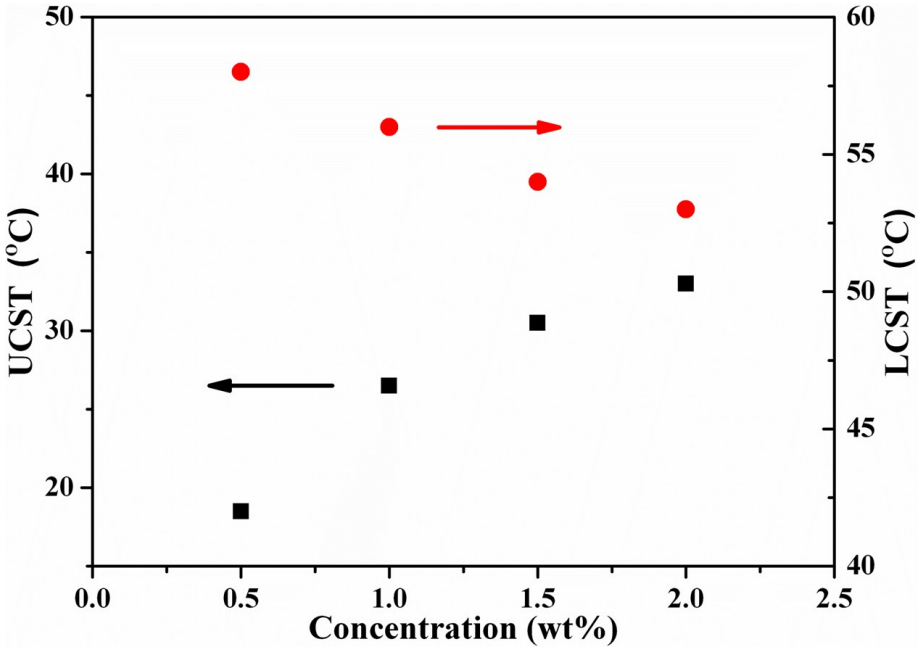

Fig. S6. Polymer concentration dependent LCST/UCST of P*t*BMA$_{329}$-*b*-P*t*BMA$_{142}$ in methanol.

9. DLS analysis of the P*t*BMA$_{329}$-*b*-PVEA$_{142}$ micelles

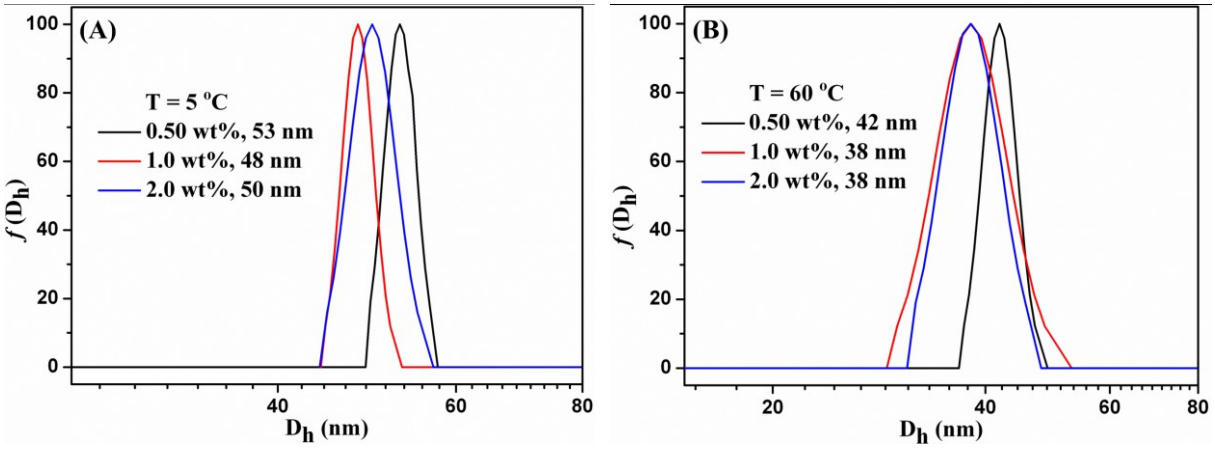

Fig. S7. The hydrodynamic diameter distribution $f(D_h)$ of the P*t*BMA@PVEA micelles formed in methanol at 5 °C (A), and the inverse PVEA@P*t*BMA micelles formed in methanol at 60 °C (B), with different polymer concentration of P*t*BMA$_{329}$-*b*-PVEA$_{142}$.

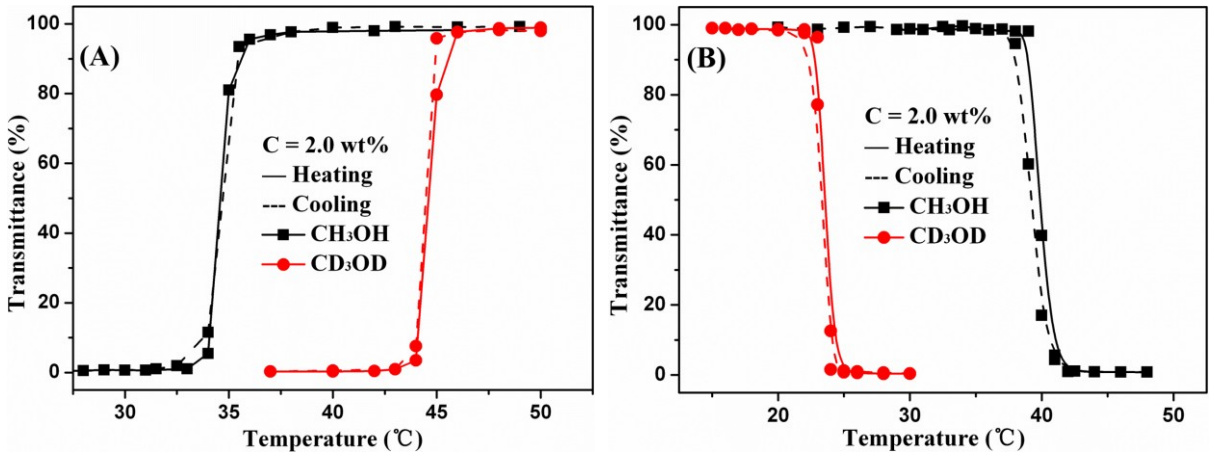

Fig. S8 The transmittance *versus* temperature plots for reference homopolymers of P*t*BMA$_{329}$ (A) and PVEA$_{133}$ (B) in methanol (CH_3OH) and in deuterated methanol-d_4 (CD_3OD).

10. TEM images of the P*t*BMA-*b*-PVEA micelles with different block chain length

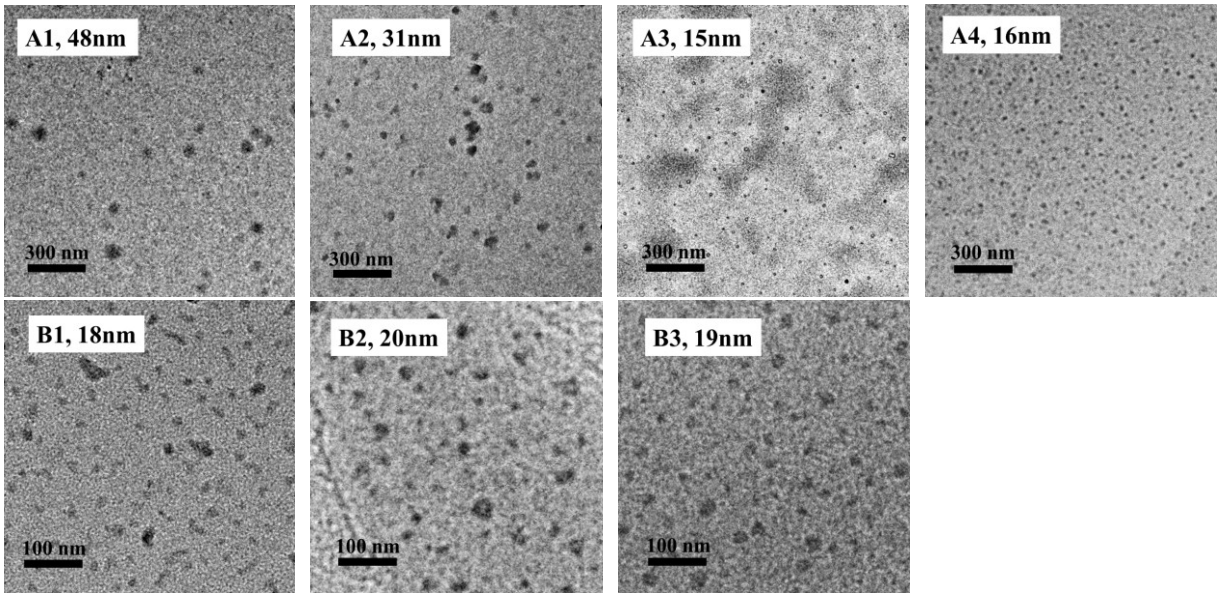

Fig. S9. TEM images of the P*t*BMA@PVEA micelles of P*t*BMA$_{217}$-*b*-PVEA$_{88}$ (A1), P*t*BMA$_{217}$-*b*-PVEA$_{136}$ (A2), P*t*BMA$_{217}$-*b*-PVEA$_{184}$ (A3), and P*t*BMA$_{217}$-*b*-PVEA$_{244}$ (A4) formed at 5 °C below the UCST of the P*t*BMA block and the inverse PVEA@P*t*BMA micelles of P*t*BMA$_{217}$-*b*-PVEA$_{136}$ (B1), P*t*BMA$_{217}$-*b*-PVEA$_{184}$ (B2) and P*t*BMA$_{217}$-*b*-PVEA$_{244}$ (B3) formed at 60 °C above the LCST of the PVEA block.